Journal of Physics: Conference Series

On the growth of Co-doped $BaFe_2As_2$ thin films on CaF_2

IOP Conf. Series: Journal of Physics: Conf. Series **1293** (2019) 012014 doi:10.1088/1742-6596/1293/1/012014

On the growth of Co-doped $BaFe_2As_2$ thin films on CaF_2

Marco Langer[1], Sven Meyer[1], Kai Ackermann[1], Lukas Grünewald[2], Sandra Kauffmann-Weiss[1], Saicharan Aswartham[3], Sabine Wurmehl[3], Jens Hänisch[1] and Bernhard Holzapfel[1]

[1] Karlsruhe Institute of Technology, Institute for Technical Physics, 76344 Eggenstein-Leopoldshafen, Germany
[2] Karlsruhe Institute of Technology, Laboratory for Electron Microscopy, 76131 Karlsruhe, Germany
[3] Leibniz Institute for Solid State and Materials Research Dresden, Institute for Solid State Research, 01171 Dresden, Germany

E-mail: marco.langer@kit.edu

Abstract. The competition between phase formation of BaF_2 and $Ba(Fe_{1-x}Co_x)_2As_2$ on CaF_2 single crystals has been analysed. $Ba(Fe_{0.92}Co_{0.08})_2As_2$ thin films have been deposited by pulsed laser deposition. X-ray diffraction, atomic force microscopy and scanning electron microscopy studies have revealed that the formation of secondary phases and misorientations as well as the growth modes of the $Ba(Fe_{0.92}Co_{0.08})_2As_2$ thin films strongly depend on the growth rate. At high growth rates, formation of BaF_2 is suppressed. The dependency of the $Ba(Fe_{0.92}Co_{0.08})_2As_2$ lattice parameters supports the idea of fluorine diffusion into the crystal structure upon suppression of BaF_2 formation similar as was proposed for $FeSe_{1-x}Te_x$ thin films on CaF_2. Furthermore, a growth mode transition from a layer growth mechanism to a three-dimensional growth mode at high supersaturation has been found, suggesting similarities between the growth mechanism of iron-based superconductors and high-T_c cuprate thin films.

1. Introduction

CaF_2 single crystalline substrates have been proven to yield *high-quality* thin films of Fe-based superconductors (FeSC), i.e. in terms of high critical temperature T_c and high critical current density J_c, grown either by pulsed laser deposition (PLD) or molecular beam epitaxy (MBE) [1]. This is especially true in the case of Co-doped $BaFe_2As_2$ (Ba122) thin films, for which $T_{c0} \sim 26\,K$ has been reported on CaF_2 [2], i.e. similar to values of annealed single crystals [3], whereas thin films grown on other substrates such as MgO, $SrTiO_3$ (STO) or $(LaAlO_3)_{0.3}(Sr_2TaAlO_6)_{0.7}$ (LSAT) often show a reduction of T_c by several Kelvin [4]. However, the phase purity of FeSC thin films remains a major challenge even ten years after the first reports [5]. The growth of FeSC thin films is often accompanied by formation of secondary phases such as FeAs or other Fe-rich phases and misoriented Ba122 grains on the sample surface [6] which impedes the development of many possible applications such as planar junction technology or sub-micrometer single-photon nanowire detectors. Additionally to these precipitates usually obtained on all kind of substrates, Ba122 thin films grown on CaF_2 often show the formation of BaF_2 [7, 8, 9]. This can be understood if one considers the thermal instability of CaF_2 under vacuum conditions at

typical deposition temperatures, T_d, of $\sim 700\,^{\circ}C$ which are necessary for the growth of epitaxial Ba122 thin films [10]. Fluorine diffusion and other interface reactions are regularly reported already at moderate $T_d \sim 300\,^{\circ}C$ [11, 12, 13], and a considerably high density of free fluorine adatoms on the substrate surface in case of $T_d \sim 700\,^{\circ}C$ is therefore likely. Contrary to the occasional reports of BaF_2 formation during the growth of Ba122 thin films, others, e.g. Yuan *et al.* [14] or Lee *et al.* [15], have reported the growth of films without apparent x-ray diffraction reflections of BaF_2. At present, the competition of the phase formation between BaF_2 and $Ba(Fe_{1-x}Co_x)_2As_2$ has never been discussed and it is not clear which film growth parameters most strongly influence the formation of BaF_2. Furthermore, the surface morphology and the growth modes of Ba122 films on CaF_2 has not been addressed apart from reports by Sobota *et al.* [16] and Daghero *et al.* [17], who found a granular three-dimensional growth mode surface on 500 nm scale [16] together with rectangular outgrowths ("terraces") of 100 nm to 200 nm length on 2 µm scale [17] for films with nominal Co content $x = 0.1$ and 0.8 respectively grown with KrF excimer laser at 700 °C and 7 Hz.

In this report, we discuss the influence of the growth rate, controlled in this study by the laser pulse energy E, on the growth of Ba122 thin films on CaF_2. It was found that the formation of BaF_2 predominantly occurs at low growth rates, whereas at high growth rates the formation of BaF_2 is suppressed. Furthermore, the suppression of BaF_2 formation coincides with pronounced lattice parameter changes, promoting the idea of fluorine diffusion into the Ba122 crystal structure, similar to what was proposed [11] for $FeSe_{1-x}Te_x$ thin films grown on CaF_2. Additionally, growth mode transitions from a $c_\perp$-oriented layer growth mechanism with terraces and a typical ledge height of $c/2$ at low supersaturation occurs to a $c_\parallel$-oriented three-dimensional growth mode with (110)-oriented grains at high supersaturation.

2. Experimental

The $Ba(Fe_{1-x}Co_x)_2As_2$ thin films with a nominal Cobalt content $x = 0.08$ have been grown by conventional on-axis pulsed laser deposition with a frequency-tripled Nd:YAG laser ($\lambda = 355$ nm, Quanta-Ray Indi-40-10, Spectra-Physics) at 10 Hz onto commercially available CaF_2 single crystals (CrysTec GmbH) with dimensions of 10 mm × 5 mm × 0.5 mm. A polycrystalline target was prepared by standard solid-state sintering as described in more detail in Ref. [18]. The substrates were radiantly heated by a resistive boron nitride heater, and the deposition temperature was calibrated by a thermocouple near the heater plate within the thermal shielding of the heater. The laser focus spot had an ellipsoidal shape with an area $A \approx 1\,\mu m^2$. The target was mounted on a target carousel and was scanned around three axes (x, y, rotation) to ensure homogenous ablation. The distance between substrate and target was 50 mm. The base pressures at room temperature and deposition temperature were 4×10^{-9} and 1×10^{-8} mbar respectively. The laser energy was varied between 12 mJ and 55 mJ (i.e. the laser fluence ε between 1.2 and 5.5 Jcm^{-2}) and was measured before and after each deposition behind the chamber through a laser exit window in order to confirm absence of an energy gradient during deposition.

X-ray diffraction was performed on a Rigaku SmartLab 3 kW (40 kV, 30 mA) 5-axis diffractometer with a goniometer radius of 300 mm, parallelized Cu-K_α radiation and a HyPix-3000 2D detector. Film thickness t for thin films ($t < 50$ nm) was calculated by analysing Kissing fringes obtained in specular x-ray reflectivity (XRR). The thickness of thicker films was estimated by assuming a constant growth rate under similar deposition parameters. Out-of-plane lattice constants c were calculated by extrapolation of measured lattice constants, obtained in symmetric $2\theta/\theta$ scans (line focus, 1D detector mode), plotted against the Nelson-Riley function $f_{NR} = 0.5(\cos\theta^2/\sin\theta + \cos\theta^2/\theta)$. Reciprocal space maps (RSM) were obtained with a point focus (PB-0.3 mm pinhole CBO and 0.3 mm-collimator) with the detector in 2D mode. In-plane orientation was proven by ϕ-scans and pole figures of the (103) reflection on selected samples. $R(T)$ dependencies of unstructured films were measured in van der Pauw

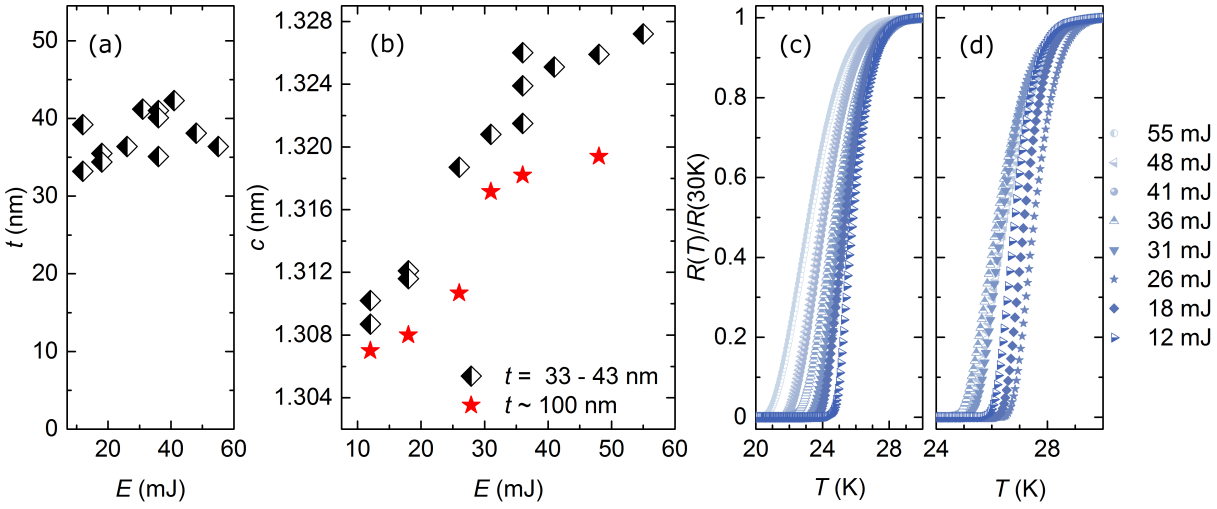

Figure 1. (a) XRR-determined film thickness vs. laser energy for the sample series with a nominal thickness $t < 50\,\text{nm}$. (b) c-axis vs. laser energy for both sample series. Normalized resistance vs. temperature for thin (c) and (d) thick samples. The highest T_c of $T_{c90} = 28.5\,\text{K}$ and $T_{c0} = 26.1\,\text{K}$ was measured for a film with a nominal thickness of 100 nm grown at $E = 26\,\text{mJ}$ ($\varepsilon = 2.6\,\text{Jcm}^{-2}$) (stars in (d)). At higher laser energies (i.e. growth rates), T_c is decreased by several Kelvin for thin and thick samples.

geometry on a Quantum Design physical properties measurement system (PPMS 14 T) with a heating rate of $1\,\text{K}\,\text{min}^{-1}$. A Keithley 2460 SourceMeter in combination with a Keithley 2182A nanovoltmeter were employed for pulsed current measurements in order to reduce the voltage noise level compared to the built-in PPMS system bridge. T_{c0} was defined as the temperature at which the voltage signal exceeded the noise level. This resistively measured T_{c0} coincided with inductively measured T_c as confirmed on selected samples by a two-coil mutual inductance method, measured with a custom-designed PPMS puck mounted with the coils. Atomic force microscopy (AFM) height and adhesion maps were obtained on a Bruker Dimension Edge AFM with ScanAsyst-Air Si/Si_3N_4 tips ($f = 70\,\text{kHz}$, $l = 0.4\,\text{N}\,\text{m}^{-1}$) in PeakForce Tapping mode and a typical scan rate of 0.1 Hz. Scanning electron microscopy (SEM) images were taken on a Zeiss Leo 1350 equipped with a field emission gun, operated at a working distance of 5 mm and an acceleration voltage of 20 kV.

A sample series with varying laser energy at $T_d = 700\,^\circ\text{C}$ with $t < 50\,\text{nm}$ has been grown in order to obtain the growth rate via x-ray reflectivity. Based on this growth rate, a second series of thicker samples with a nominal thickness of $t \sim 100\,\text{nm}$ has been grown by adjusting the number of laser pulses.

3. Results

The thin samples grown for determination of the growth rate have a thickness ranging from 33 nm to 45 nm (figure 1(a)). The growth rate varied between $\sim 0.4\,\text{Å}\,\text{s}^{-1}$ for films grown at a laser pulse energy of 12 mJ and $\sim 0.9\,\text{Å}\,\text{s}^{-1}$ grown at 55 mJ. The out-of-plane lattice parameter c of both sample series shows a pronounced dependency on the laser fluence with an onset of a plateau at high laser fluence (figure 1(b)). All samples have lattice parameters bigger than the lattice parameters of single crystals with the same nominal Co content, indicating an elongation of the tetragonal unit cell along the c direction. Furthermore, the lattice parameters depend on the film thickness, where in general thicker films have lattice parameters closer to bulk values.

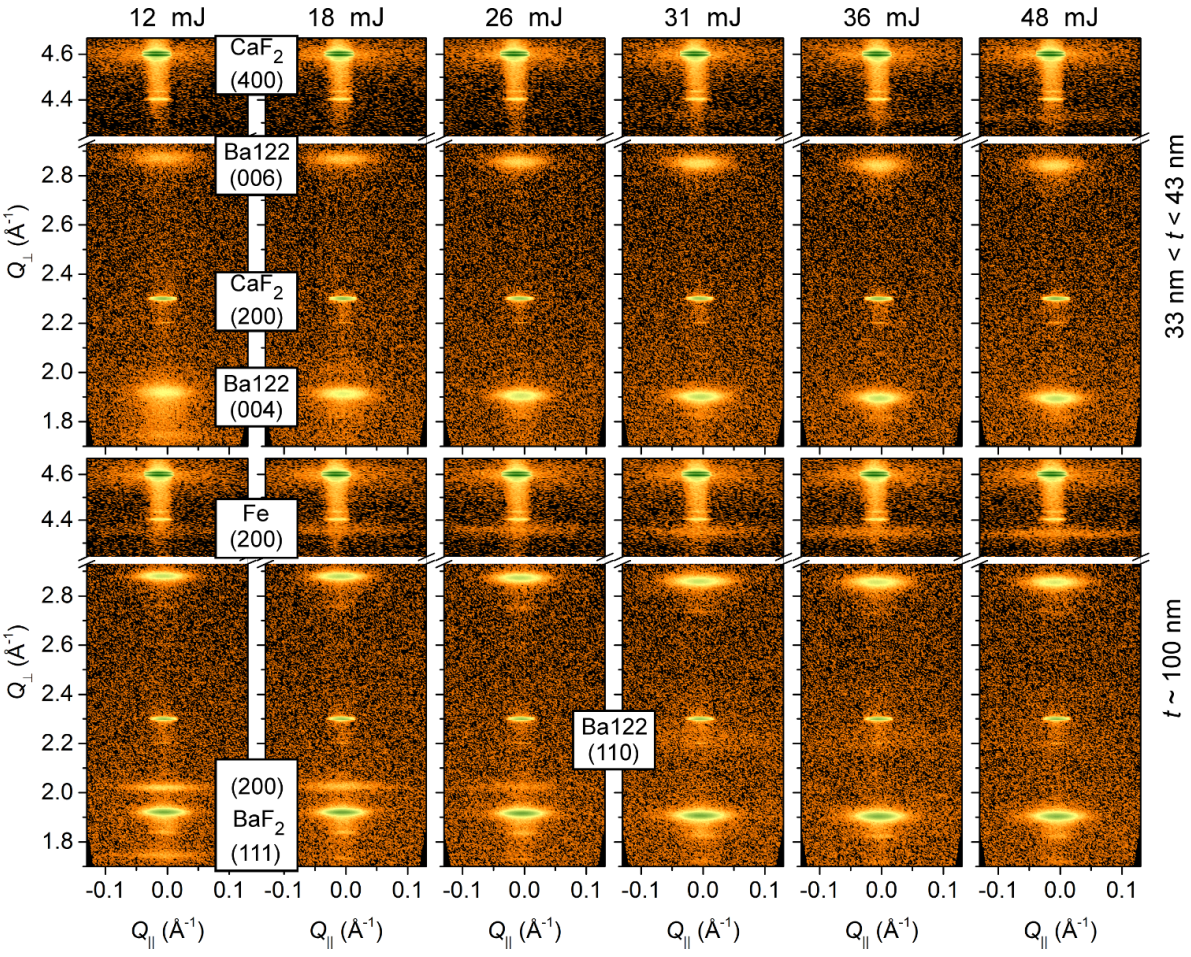

Figure 2. Reciprocal space maps of symmetric $2\theta/\theta$ scans around Ba122(004) ($Q_\perp \sim 1.9\,\text{Å}^{-1}$), Ba122(006) ($Q_\perp \sim 2.85\,\text{Å}^{-1}$) and CaF_2(400) ($Q_\perp \sim 4.6\,\text{Å}^{-1}$) of thin ($33\,\text{nm} < t < 43\,\text{nm}$, top) and thicker ($t \sim 100\,\text{nm}$, bottom) samples grown at laser energies of 12 mJ, 18 mJ, 26 mJ, 31 mJ, 36 mJ and 48 mJ (from left to right).

T_{c0} varied between 19.6 K and 23.7 K for thin and between 23.5 K and 26.1 K for thick samples with a nominal thickness of $t \sim 100\,\text{nm}$ (figure 1(c) and (d)). The highest T_c values were obtained on films grown at moderate laser energies of 12 mJ to 30 mJ, i.e. at laser fluences of $1.2\,\text{Jcm}^{-2}$ to $3.0\,\text{Jcm}^{-2}$. For both sample series, films grown at $E > 30\,\text{mJ}$ showed a reduction in T_c by several Kelvin.

X-ray diffraction using reciprocal space maps (RSM) (figure 2) revealed that all samples contain one or more secondary phases or orientations, such as BaF_2 ((111) at $Q_\perp \sim 1.74\,\text{Å}^{-1}$ and (200) at $Q_\perp \sim 2.02\,\text{Å}^{-1}$), (110)-oriented Ba122 ($Q_\perp \sim 2.19\,\text{Å}^{-1}$) and Fe-rich precipitates (Fe(200) at $Q_\perp \sim 4.34\,\text{Å}^{-1}$). BaF_2 reflections are visible for laser energies $E \leq 31\,\text{mJ}$, whereas the formation of Fe-rich precipitates is increased at high laser energy. The formation of (110)-oriented Ba122 is only apparent for samples with a sufficient thickness ($t \sim 100\,\text{nm}$), as indicated by a broad, low-intensity reflection in case of laser energies $E \geq 36\,\text{nm}$.

Films grown at low laser energy, e.g. 12 mJ, contain granular precipitates at their surface with a maximal lateral size of $\sim 170\,\text{nm}$ and a height of $\leq 40\,\text{nm}$ (figure 3(a), (d), (g) and (j)).

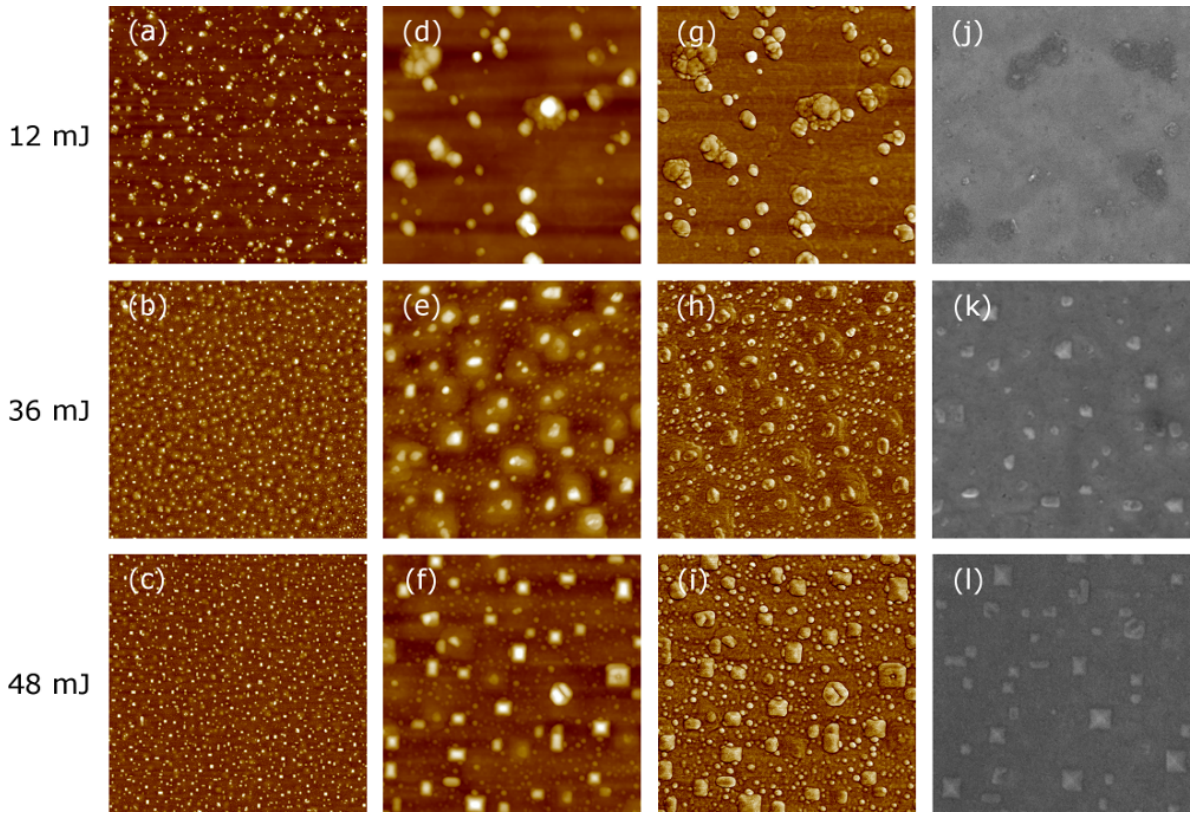

Figure 3. Representative surface morphologies of three thin samples (33 nm $< t <$ 43 nm) grown at 12 mJ (top), 36 mJ (middle) and 48 mJ (bottom). (a) - (c) 5 µm × 5 µm AFM height maps. (d) - (f) 1 µm × 1 µm AFM height maps. (g) - (i) 1 µm × 1 µm AFM adhesion maps. (j) - (l) 1 µm × 1 µm SEM micrographs.

Apart from these precipitates, the film surface is rather flat and a layer growth mechanism with a ledge height of $c/2$ is visible (figure 3(g)). A detailed determination of ledge width and shapes is often complicated due to the high density of the granular precipitates. Films grown at high laser energy, e.g. 48 mJ, show a completely different surface morphology (figure 3(c), (f), (i) and (l)). The granular precipitates are absent but a high density of square pyramids or rectangular platelets with a lateral size of $\sim 50\,\text{nm} \times 50\,\text{nm}$ and a height of $\leq 20\,\text{nm}$, predominantly oriented along $CaF_2[100]$, are visible. Films with a thickness of $t < 50\,\text{nm}$ often show a higher density of pyramids compared to the elongated platelets as can be seen in figure 3, whereas thicker films $t \geq 100\,\text{nm}$ show a similar or even higher density of the elongated flat platelets. Similar to the form of the terraces in case of low laser energy, the shape of these $CaF_2[100]$-oriented precipitates is often better visible in the AFM adhesion maps rather than in the AFM height maps. In contrast to the $c/2$ terraces observed on films grown at low laser energy, the layer growth mechanism is absent for films grown at high laser energy and the surface of such films contains a high density of three-dimensional islands (figure 3(i)). Films grown at an intermediate laser energy, e.g. 36 mJ, exhibit a mixture of both kinds of precipitates discussed above (figure 3(b), (e), (h) and (k)).

The growth mode transition from a layer growth mechanism with terraces to a three-dimensional growth mode without terraces occurs within a rather small energy range, as can be seen exemplary in the AFM adhesion maps for two thick samples grown at $E = 31\,\text{mJ}$ (figure

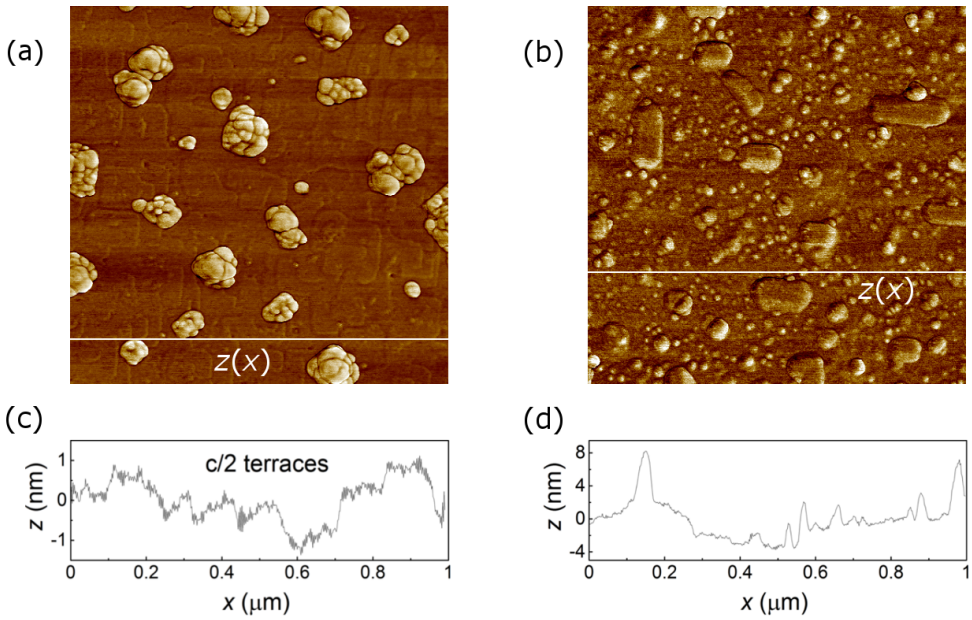

Figure 4. Surface morphology of two thick films ($t \sim 100\,\mathrm{nm}$) grown at $E = 31\,\mathrm{mJ}$ (a, c) and $E = 36\,\mathrm{mJ}$ (b, d). (a, b) $1\,\mu\mathrm{m} \times 1\,\mu\mathrm{m}$ AFM adhesion maps. (c, d) Extracted line scans of the associated AFM height maps as indicated by the white lines in (a, c). A transition between quasi-2D terraced growth and 3D island growth is clearly visible.

4(a)) and $E = 36\,\mathrm{mJ}$ (figure 4(b)). Whereas the former film exhibits terraces with a ledge height of $c/2$ and a ledge width of $\sim 50 - 100\,\mathrm{nm}$ (figure 4(c)), the terraces are absent in the latter case and the surface roughness increased significantly (figure 4(d)).

4. Discussion

The highest $T_{c0} \sim 26.1\,\mathrm{K}$ obtained on films with $t \sim 100\,\mathrm{nm}$ is comparable to the highest reported T_{c0} for Ba122 thin films by Tarantini *et al.* [2]. The reduction of T_c by several Kelvin for films with a thickness of $33\,\mathrm{nm} < t < 43\,\mathrm{nm}$ is in good agreement with the thin films grown by Yuan *et al.* [19]. The strong dependency of the lattice parameters, secondary phase formation, surface morphology and critical temperature T_c on the laser fluence, i.e. growth rate, has not been discussed so far by others, but may serve as an explanation for the contradictory published results [7, 9, 15, 19], namely the strong variation in lattice parameters and formation of BaF_2 in some cases. The c-axis lattice parameter in the range $1.307\,\mathrm{nm} \leq c \leq 1.327\,\mathrm{nm}$ of this study provides an explanation for the strong variation of reported lattice parameters, i.e. from $1.303\,\mathrm{nm}$ [19] to $1.319\,\mathrm{nm}$ [7]. In addition to the dependency on the film thickness and growth rate, we have found that the c-axis lattice parameter also strongly depends inversely on the deposition temperature, i.e. it decreases at increasing deposition temperature. These results will be published elsewhere. Films without BaF_2 precipitates show a stronger elongation of the unit cell along the c-axis compared to films which contain BaF_2 precipitates. This correlation between BaF_2 formation and changes in lattice parameters in case of BaF_2 phase formation suppression at high growth rates supports the idea of a fluorine diffusion into the Ba122 crystal structure similar as was already discussed for $FeSe_{1-x}Te_x$ thin films grown on CaF_2 [11]. The granular precipitates found on film surfaces for which x-ray analysis shows the formation of BaF_2 have similar lateral dimensions as the BaF_2 precipitates found in Ni-doped $BaFe_2As_2$

films on CaF_2 [8] and are thereby most likely BaF_2 precipitates as well. Ongoing TEM analysis will clarify the different fluorine distribution on selected films grown at different growth rates. The CaF_2[100]-oriented pyramidal precipitates are most likely (110)-oriented Ba122 grains as suggested by x-ray analysis. This interpretation is further supported by measurements of (110)-pole figures (not shown here) as well as previous TEM analysis on Ba122 films grown on MgO, for which these characteristic pyramids were also detected and identified as misoriented Ba122.

At present, it is not fully clear whether the growth mode transition from a layer growth mechanism with $c/2$ ledge heights to a three-dimensional growth with (110)-oriented precipitates is misfit-driven, supersaturation-driven or a mixture of both. Since the suggested fluorine diffusion into the Ba122 crystal structure upon increase of the growth rate changes the lattice parameters, the misfit between the substrate and the film most likely varies for the samples grown at different laser energies. Contrariwise, a supersaturation-driven growth mode transition from $c_\perp$- to $c_\parallel$-oriented growth at high supersaturation is well known from the growth of high-T_c cuprate thin films [20]. This transition is commonly attributed to the anisotropy of the surface Gibbs energies [21]. At low supersaturation, the critical nuclei reduce their surface energies by assuming c-axis orientation [22]. At present, films on other, fluorine-free, substrates are deposited and analysed in order to disentangle these two possible explanations. The formation of (110)-oriented Ba122 grains on the film surface depends, similar to the lattice parameters, inversely on the growth temperature, as will be discussed elsewere. At $T_\mathrm{d} \geq 720\,^\circ\mathrm{C}$, no (110)-reflection was found in XRD, again in good agreement with the suppression of a-axis growth in case of cuprate films at high deposition temperature, i.e. at low supersaturation [23].

5. Conclusions

In summary, we have shown that the formation of BaF_2, the Ba122 lattice parameters and the surface morphology for films grown on CaF_2 strongly depend on the growth rate. Suppression of BaF_2 phase formation is achieved at high growth rates and coincides with an elongation of the unit cell along the c-axis, supporting the idea of fluorine diffusion into the Ba122 crystal structure being one of the main reasons for the commonly reported increased c-axis parameters for films grown on CaF_2. Since all films in this study were grown at the same deposition temperature, the influence of the thermal mismatch between the film and the CaF_2 substrate, usually attributed as the cause of the distortion of the Ba122 unit cell, has to be considered with care. A growth mode transition from a $c_\perp$-oriented layer growth mechanism with ledge heights of $c/2$ to a three-dimensional growth mode with $c_\parallel$-oriented Ba122 grains on the film surface occurs almost simultaneously at high supersaturation. Ongoing work will clarify the origin of this transition, whether it is linked to fluorine diffusion into the Ba122 crystal structure upon suppression of BaF_2 or can be explained similarly as the supersaturation-driven transitions well known for cuprate high-T_c thin films.

References

[1] Imai Y, Nabeshima F and Maeda A 2017 *Condensed Matter* **2** 25
[2] Tarantini C, Kametani F, Lee S, Jiang J, Weiss J D, Jaroszynski J, Hellstrom E E, Eom C B and Larbalestier D C 2014 *Scientific Reports* **4**
[3] Sun D, Xiao J and Lin C 2011 *Journal of Crystal Growth* **321** 55–59
[4] Haindl S, Kidszun M, Onken F, Mietke A and Thersleff T 2013 *International Journal of Modern Physics B* **27** 1330001
[5] Katase T, Hiramatsu H, Yanagi H, Kamiya T, Hirano M and Hosono H 2009 *Solid State Communications* **149** 2121–2124
[6] Katase T, Hiramatsu H, Kamiya T and Hosono H 2012 *Superconductor Science and Technology* **25** 084015
[7] Kurth F, Reich E, Hänisch J, Ichinose A, Tsukada I, Hühne R, Trommler S, Engelmann J, Schultz L, Holzapfel B and Iida K 2013 *Applied Physics Letters* **102** 142601
[8] Richter S, Kurth F, Iida K, Pervakov K, Pukenas A, Tarantini C, Jaroszynski J, Hänisch J, Grinenko V, Skrotzki W, Nielsch K and Hühne R 2017 *Applied Physics Letters* **110** 022601

[9] Iida K, Grinenko V, Kurth F, Ichinose A, Tsukada I, Ahrens E, Pukenas A, Chekhonin P, Skrotzki W, Teresiak A, Hühne R, Aswartham S, Wurmehl S, Mönch I, Erbe M, Hänisch J, Holzapfel B, Drechsler S L and Efremov D V 2016 *Scientific Reports* **6**
[10] Haindl S, Hanzawa K, Sato H, Hiramatsu H and Hosono H 2016 *Scientific Reports* **6**
[11] Ichinose A, Nabeshima F, Tsukada I, Hanawa M, Komiya S, Akiike T, Imai Y and Maeda A 2013 *Superconductor Science and Technology* **26** 075002
[12] Zarraga-Colina J, Nix R M and Weiss H 2005 *The Journal of Physical Chemistry B* **109** 10978–10985
[13] Qiu W, Ma Z, Patel D, Sang L, Cai C, Hossain M S A, Cheng Z, Wang X and Dou S X 2017 *ACS Applied Materials & Interfaces* **9** 37446–37453
[14] Yuan P, Xu Z, Wang D, Zhang M, Li J and Ma Y 2016 *Superconductor Science and Technology* **30** 025001
[15] Lee J, Jiang J, Kametani F, Oh M J, Weiss J D, Collantes Y, Seo S, Yoon S, Tarantini C, Jo Y J, Hellstrom E E and Lee S 2017 *Superconductor Science and Technology* **30** 085006
[16] Sobota R, Plecenik T, Gregor M, Truchly M, Satrapinskyy L, Vidis M, Secianska K, Kurth F, Holzapfel B, Iida K, Kus P and Plecenik A 2014 *Applied Surface Science* **312** 182–187
[17] Daghero D, Pecchio P, Laviano F, Gonnelli R, Kurth F, Grinenko V and Iida K 2014 *Applied Surface Science* **312** 23–29
[18] Kurth F, Iida K, Trommler S, Hänisch J, Nenkov K, Engelmann J, Oswald S, Werner J, Schultz L, Holzapfel B and Haindl S 2013 *Superconductor Science and Technology* **26** 025014
[19] Yuan P, Xu Z, Li C, Quan B, Li J, Gu C and Ma Y 2017 *Superconductor Science and Technology* **31** 025002
[20] Pennycook S, Chisholm M, Jesson D, Feenstra R, Zhu S, Zheng X and Lowndes D 1992 *Physica C: Superconductivity* **202** 1–11
[21] Granozio F M and di Uccio U S 1997 *Journal of Alloys and Compounds* **251** 56–64
[22] Granozio F M, Salluzzo M, di Uccio U S, Maggio-Aprile I and Fischer Ø 2000 *Physical Review B* **61** 756–765
[23] Jeschke U, Schneider R, Ulmer G and Linker G 1995 *Physica C: Superconductivity* **243** 243–251